AGU ADVANCING EARTH AND SPACE SCIENCE

Geophysical Research Letters

RESEARCH LETTER
10.1029/2020GL090768

Key Points:

- Changes in alongshore wind stress are insufficient to obtain overall changes in the California Current System (CCS) upwelling in the CESM1 large ensemble
- Changes in geostrophic transport make a substantial contribution to changes in the CCS upwelling
- A combination of changes in Ekman and geostrophic transports reproduces overall changes in the CCS upwelling

Supporting Information:

- Supporting Information S1

Correspondence to:
H. Ding,
hui.ding@noaa.gov

Citation:
Ding, H., Alexander, M. A., & Jacox, M. G. (2021). Role of geostrophic currents in future changes of coastal upwelling in the California Current System. *Geophysical Research Letters*, *48*, e2020GL090768. https://doi.org/10.1029/2020GL090768

Received 10 SEP 2020
Accepted 18 DEC 2020

Role of Geostrophic Currents in Future Changes of Coastal Upwelling in the California Current System

Hui Ding[1,2], Michael A. Alexander[2], and Michael G. Jacox[2,3]

[1]CIRES, University of Colorado, Boulder, CO, USA, [2]NOAA Physical Sciences Laboratory, Boulder, CO, USA, [3]NOAA Southwest Fisheries Science Center, Monterey, CA, USA

Abstract Given the importance of coastal upwelling in the California Current System (CCS), there is a considerable interest in predicting its response to global warming. However, upwelling changes are often treated as synonymous with changes in upwelling-favorable winds, while the role of geostrophic transport is unaccounted for. Here, we examine the respective roles of Ekman and geostrophic transports using the Community Earth System Model Large Ensemble. In some parts of the CCS, the contribution of geostrophic transport to long-term changes in upwelling is equal or greater than the contribution from Ekman transport. The combination of the two transports nearly close the momentum budget, and thus reproduce the mean state, interannual variability, and long-term changes in upwelling. These results highlight the importance of accounting for ocean circulation when quantifying upwelling and its variability and change.

Plain Language Summary The California Current System (CCS) is an eastern boundary current system along the west coast of North America. The CCS hosts a diverse marine ecosystem and a high level of production for commercially valuable fish. Upwelling delivers deep, nutrient-rich water to the sunlit surface, which provides nutrients that stimulate phytoplankton growth, fueling the marine ecosystem. Thus, potential future changes in coastal upwelling are of concern for the health of the CCS ecosystem, the livelihood of fishers, and food security. To date, projections of upwelling change have focused primarily on modifications of the wind-driven (Ekman) transport. However, a second component of the ocean circulation, the geostrophic transport, can also impact coastal upwelling. In this study, we investigate the roles of both transport components in coastal upwelling change under global warming. We find that changes in the geostrophic currents, which have been neglected in many previous studies, make a substantial contribution to overall changes in the CCS coastal upwelling.

1. Introduction

The California Current System (CCS) is one of the world's major eastern boundary upwelling systems. In this region, coastal upwelling transports deep, nutrient-rich water to the sunlit surface, which provides nutrients for phytoplankton and maintains a productive ecosystem, with diverse populations of commercially valuable fish near the United States west coast (Rykaczewski & Checkley, 2008; Ryther et al., 1969). Therefore, projecting the response of the CCS upwelling to greenhouse gas warming is of great ecological and socioeconomic importance.

It is often assumed that wind-driven cross-shore Ekman transport is the sole driver of coastal upwelling in the CCS and other eastern boundary upwelling systems (e.g., Huyer, 1983), and the first upwelling indices treated cross-shore Ekman transport as being equivalent to vertical transport (Bakun, 1973, 1975). Extending this assumption to future change, Bakun (1990) hypothesized that the cross-shore atmospheric sea level pressure gradient will intensify in response to ongoing global warming, which will accelerate alongshore wind stress and increase upwelling in the CCS as well as in other eastern boundary upwelling systems. Bakun's hypothesis has stimulated a number of investigations of wind forcing in a changing climate using historical observational records and outputs of coupled atmosphere-ocean general circulation models (e.g., Cardone et al., 1990; Garcia-Reyes & Largier, 2010; Garcia-Reyes et al., 2015; Hsieh & Boer, 1992; Mote & Mantua, 2002; Narayan et al., 2010; Rykaczewski et al., 2015; Sydeman et al., 2014; Wang et al., 2015). For the CCS, Garcia-Reyes and Largier (2010) suggested an intensified trend in wind forcing during March-July over the years 1982–2008 off the central California coast, and Narayan et al. (2010) found an intensification

of the alongshore wind stress during 1960–2001 along most of the California coast. Rykaczewski et al. (2015) found that projected changes are heterogeneous, with most of the models from the fifth phase of the Coupled Model Intercomparison Project (CMIP5) projecting a significant reduction of the alongshore wind stress in the southern part of the CCS and a slight intensification in the northern part during June-August.

However, Ekman theory provides an incomplete dynamical interpretation for coastal upwelling and a key omission is cross-shore geostrophic transport, which is an important component in eastern boundary upwelling systems (Marchesiello & Estrade, 2010), including Peru (Colas et al., 2008; Huyer et al., 1987), Western Australia (McCreary et al. 1986), New Caledonia (Marchesiello & Estrade, 2010), Benguela (Veitch et al., 2010), and California (Jacox et al., 2018). In eastern boundary current systems, alongshore sea level gradients induce near-surface geostrophic flow that is perpendicular to the coast. Since there can be no transport across the coastal boundary, the cross-shore geostrophic flow is compensated by vertical transport, which can either suppress or enhance upwelling depending on the direction of the flow (e.g., Jacox et al., 2018; Marchesiello & Estrade, 2010). In the CCS, the mean geostrophic transports are offshore (upwelling-favorable) in the northern CCS and onshore (downwelling-favorable) in the southern CCS (Figure S1a). Significant changes in sea surface height (SSH) are projected to occur in the North Pacific under global warming (Yin, 2010, 2012), which may induce changes in geostrophic transport and thus coastal upwelling. Therefore, alongshore wind stress is limited as a proxy when examining future changes in coastal upwelling. A few studies have examined the CCS coastal upwelling directly from the vertical velocity field (e.g., Brady et al., 2017; Jacox et al., 2014; Marchesiello & Estrade, 2010), but how changes in geostrophic transport contribute to changes in upwelling remains to be examined.

The monthly response of vertical transport and upwelling-favorable alongshore wind stress off the United States west coast to external radiative forcing, calculated from the Community Earth System Model Large Ensemble (CESM-LE, see Section 2), is shown in Figure 1. Changes in the alongshore wind stress do not match changes in the vertical transport (Figure 1), especially south of 35°N and north of 40°N. In the central CCS, the changes in the alongshore wind stress underestimate the magnitude of the changes in upwelling. This wind-upwelling mismatch suggests that other mechanisms induce changes in CCS upwelling, motivating us to diagnose the role of geostrophic and Ekman currents in the response of the CCS coastal upwelling to greenhouse gas warming.

2. Data and Method

2.1. Simulations and Analysis Method

We use monthly mean data from all 40 ensemble members of the CESM-LE project (Kay et al., 2015). They differ only slightly in their initial atmospheric conditions in January 1920, and are subject to identical historical radiative forcing over the years 1920–2005 and then RCP8.5 radiative forcing (the only scenario used in the CESM-LE) over the years 2006–2100 (Riahi et al., 2011). The atmospheric model has a horizontal resolution of approximately 1° × 1° in longitude and latitude and 30 vertical levels. The ocean model is Parallel Ocean Program version 2 (POP2; Smith et al., 2010) with a horizontal resolution of approximately 1° × 1°. The horizontal grid structure off the US west coast is shown in Brady et al. (2017). The POP2 has a vertical resolution of 10 m in the upper 250 m and thus well resolves the Ekman layer. One benefit of using CESM-LE is that anthropogenic-forced signals, given by the ensemble mean, can be distinguished from internal variability (Deser et al., 2012, 2014; Kay et al., 2015), which induces changes in the CCS upwelling on interannual to decadal timescales (Brady et al., 2017; Chhak & Di Lorenzo, 2007; Di Lorenzo et al., 2008; Jacox et al., 2014).

Data from the CESM-LE have been widely employed in climate studies (e.g., Deser et al., 2016; Lovenduski et al., 2016). In general, the CESM-LE has high fidelity in simulating the climatological mean states in the Pacific and North America sector (Kay et al., 2015). For example, the CESM-LE reproduces the main characteristics of the North Pacific High (NPH) during April-September, including its position and seasonality, although the model overestimates the strength of the NPH (Figure S2), which is a common problem in climate models (Li et al., 2012). In addition, the CESM-LE also well simulates the thermal low-pressure system over the southwest of the United States, which is a key driver of the alongshore wind stress. Accordingly, the CESM-LE reproduces the seasonality and magnitude of the monthly mean alongshore winds

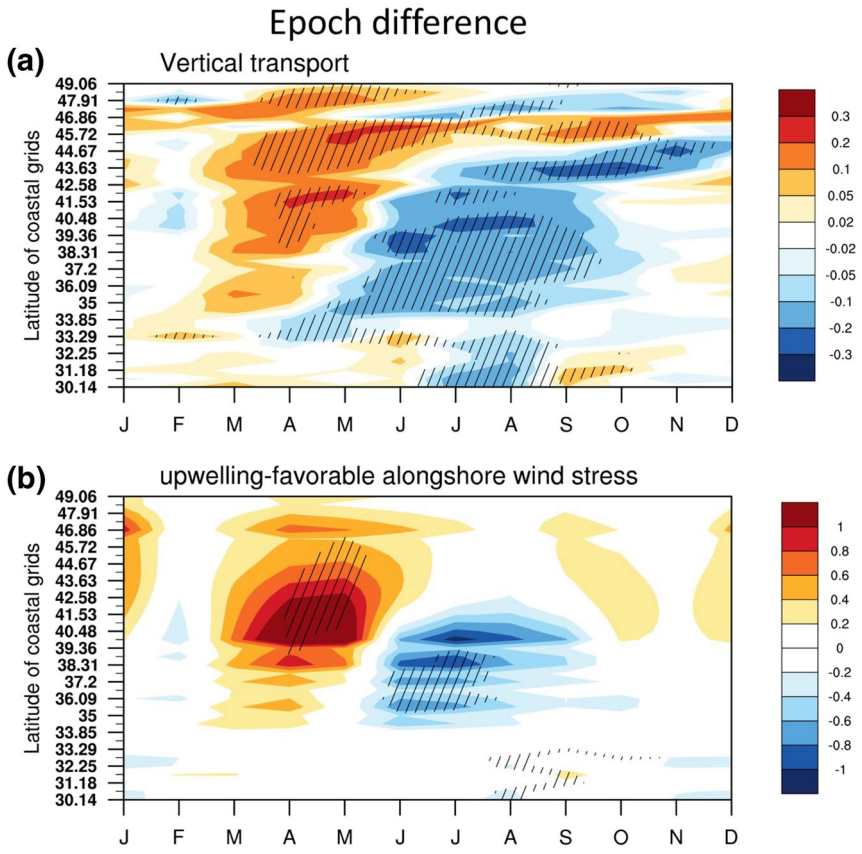

Figure 1. Monthly epoch difference (2071–2100 minus 1925–1954) in (a) vertical transport at 30-m depth and (b) upwelling-favorable alongshore wind stress. The abscissa shows the calendar month, and the ordinate shows the actual latitudes of the coastal grid. The first offshore grid cells at 30°N–49°N are considered here. Hatching indicates 95% significance. The units of vertical transport and wind stress are m^2/s and 10^{-2} N/m^2, respectively. Three consecutive grid cells are used to obtain an angle of coastline, on which wind stress is projected to obtain the upwelling-favorable component.

near California (Figure 1b in Brady et al., 2017), despite the coarse horizontal resolution of the atmospheric model. In the ocean, the CESM-LE reproduces the main characteristics of the climatological SSH along the coast (Figure S1), indicating its ability to reproduce spatiotemporal variability in the cross-shore geostrophic transport, though a stronger alongshore sea level gradient from July to October is expected to induce an overestimation of the cross-shore geostrophic transport (see Section 2.2). We note that the ocean resolution is insufficient to resolve the cross-shore upwelling zone, resulting in unrealistically weak and diffuse coastal upwelling (Estrade et al., 2008)—a common problem in global climate models (e.g., Large & Danabasoglu, 2006). To accommodate this known limitation, rather than quantifying vertical velocity or the spatial structure of Ekman and geostrophic transports, we focus on the cross-shore integrated vertical transport, for which CESM-LE agrees well with a regional ocean model with an order of magnitude higher resolution (Figure 2a cf. Jacox et al., 2018, Figure 3f). Nonetheless, our findings could be confirmed and expanded upon through dynamical downscaling of future projections using regional ocean models (Xiu et al., 2018).

Following Brady et al. (2017), an epoch difference X^i between 1925–1954 and 2071–2100 is calculated to quantify the future change, where i indicates ensemble member and X can be alongshore wind stress, vertical transport at the bottom of the climatological mean mixed layer, contributions of Ekman and geostrophic transports to the vertical transport, and other quantities. The first 6 years of the CESM simulations are omitted to avoid artificial reduction in ensemble spread, and the last three decades are used because anthropogenic-forced changes tend to emerge by the second half of the 21st century (Brady et al., 2017). The ensemble mean epoch difference, given by $\underline{X} = \sum_{i=1}^{40} X^i / 40$, represents changes due to external radiative

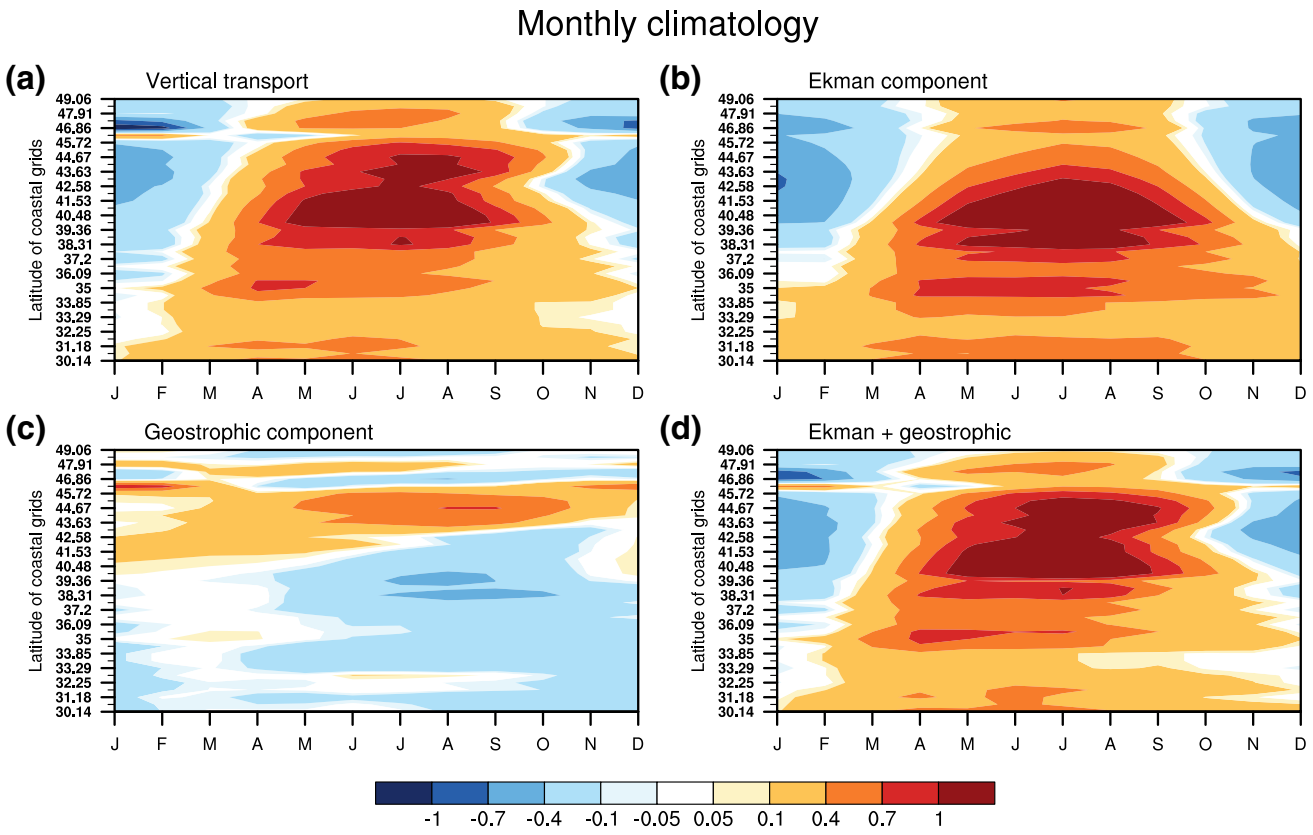

Figure 2. Monthly climatology for the years 1920–2100 of (a) vertical transport at 30-m depth (b) Ekman and (c) geostrophic components of the vertical transport, and (d) the combination of the Ekman and geostrophic components. The unit is m^2/s.

forcing. Deviations of each ensemble member from the ensemble mean arise from noise (internal climate variability). Therefore, a signal-to-noise ratio (SNR) is given by $SNR = \frac{\underline{X}}{\sigma}$, where σ is the standard deviation of internal variability. A SNR ≥2 indicates that the forced change $\underline{X}$ is significant with 95% confidence level or higher (Brady et al., 2017; Deser et al., 2014).

2.2. Contributions of Ekman and Geostrophic Transports to Coastal Upwelling

In this study, vertical, Ekman, and geostrophic transports in CESM are calculated along the North American west coast at latitudes of 30°N–49°N. Vertical transport at 30 m depth is retrieved from the first offshore grid cell as a direct measure of modeled coastal upwelling. The 30 m depth is representative of the space-time mean mixed layer depth (MLD), which is a proxy for the Ekman depth (e.g., Jacox et al. 2018). The zonal and meridional Ekman volume transports per unit length are given by $U^{Ek} = \frac{\tau^y}{f\rho}$ and $V^{Ek} = -\frac{\tau^x}{f\rho}$, respectively, where τ^x and τ^y are zonal and meridional surface wind stress, f is the Coriolis parameter, and ρ is a reference density for seawater. Zonal and meridional near-surface geostrophic volume transports per unit length are given by $U^{geo} = -\frac{gD}{f}\frac{\partial \eta}{\partial y}$ and $V^{geo} = \frac{gD}{f}\frac{\partial \eta}{\partial x}$, respectively, where g is the gravitational acceleration, D is the Ekman (mixed layer) depth, and η is the SSH. These expressions assume barotropic geostrophic transport (i.e., geostrophic velocity is uniform throughout the Ekman layer). For grid cells next to the coast, Ekman and geostrophic transports are calculated for each side of the grid cells in the analysis domain, except for the side representing the coastline, where transports are zero. Thus, contributions from both the alongshore winds and the wind stress curl are included implicitly. However, we do not explicitly

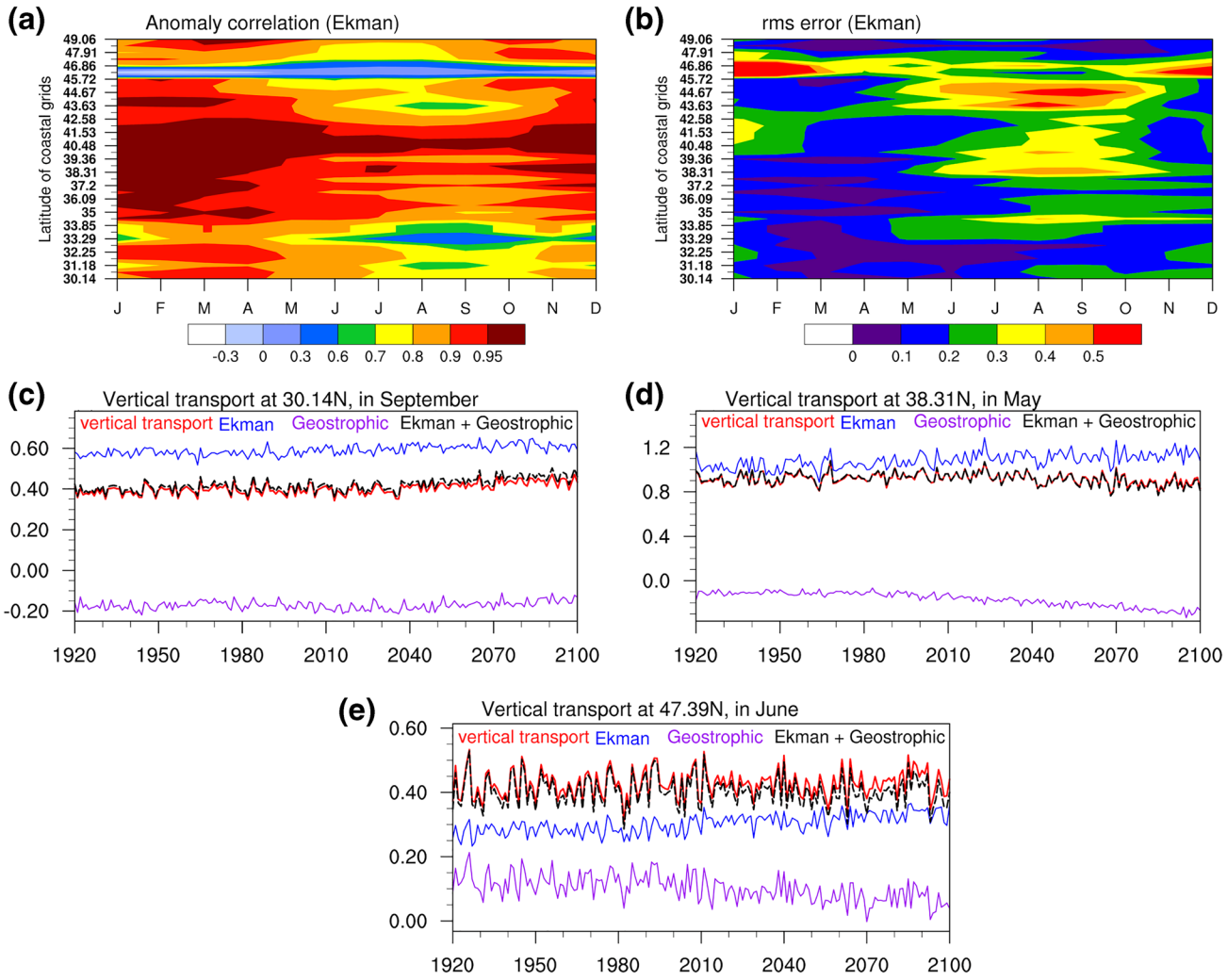

Figure 3. (a) Anomaly correlation (after removing monthly climatology) and (b) full-field root-mean-square error between vertical transport at 30m depth and Ekman component of the vertical transport. Data during 1920–2100 are used. (c–e) Temporal evolution of the ensemble-mean vertical transport and the corresponding Ekman and geostrophic components from three month-latitude pairs. The anomaly correlation coefficient between the vertical transport and the Ekman component (the sum of Ekman and geostrophic components) is 0.70 (0.99), 0.93 (0.99) and 0.63 (0.99) in (c–e), respectively.

quantify the curl-driven component of the upwelling; CESM's resolution is inadequate to resolve mesoscale changes in the wind stress curl, and the coastal and curl-driven upwelling components are not spatially separable as they co-occur in the coastal upwelling band (e.g., Capet et al. 2004). The vertical transport components attributable to Ekman and geostrophic transports are denoted as W_{ekman} and W_{geo}, respectively, while the vertical transport obtained directly from the ocean model in CESM-LE is denoted by W. As in Jacox et al. (2018), transport is calculated per meter of coastline, with units of m^2/s.

While prior analytical and modeling studies have explored the vertical and horizontal structure of upwelling and its dependence on factors such as stratification and bottom topography (e.g., Jacox and Edwards, 2011; Lentz and Chapman, 2006; Marchesiello & Estrade, 2010; Rossi et al., 2013), here we focus on integrated transports, assuming that to first order coastal upwelling is dictated by the Ekman and geostrophic transports. By integrating transports over a fixed 30 m depth, we do not account for seasonal MLD changes (Jacox et al. 2018) or the role of upwelling depth in mediating a nonlinear relationship between upwelling intensity and the strength of onshore geostrophic flow (Marchesiello & Estrade, 2010). However, examination of the momentum budget shows that across latitudes, seasons, and years, our approximation is sufficiently robust for the analysis at hand. Relative to the 50 m integration depth used by Brady et al. (2017), the 30 m

depth exhibits similar monthly climatologies and anthropogenic-forced signals (not shown), but more effectively closes the momentum budget.

3. Results

We now examine the respective contributions of Ekman and geostrophic transports to vertical transport in the monthly climatology of the CESM-LE (Figure 2). The climatological seasonal cycle of W_{ekman} is similar to that of W in both phase and magnitude (Figures 2a and 2b), indicating that Ekman transport is the primary forcing for coastal upwelling, consistent with previous studies (e.g., Bakun, 1973; Huyer, 1983). However, there are also notable differences between W and W_{ekman} (Figures 2a and 2b). For example, W_{ekman} overestimates W by 0.1 m^2/s south of about 41°N, and underestimates W by 0.4 m^2/s between 41°N and 45°N. Therefore, Ekman transport is not the only driver of coastal upwelling.

Geostrophic transport also plays a role in modulating the climatological seasonal cycle of coastal upwelling, although the contribution from geostrophic transport is less than that from Ekman transport. The difference between W and W_{ekman} (not shown) closely resembles W_{geo} (Figure 2c). South of 40°N, W_{geo} is downwelling-favorable with magnitude of 0.1–0.4m^2/s from April to January. Near 41°N, W_{geo} is upwelling-favorable during January-June and then downwelling favorable in the other months. Between about 42° and 46°N, W_{geo} augments coastal upwelling by ~0.4 m^2/s throughout the year. North of 46°N, W_{geo} has a magnitude of at least 0.1 m^2/s, but its sign varies with latitude and month. Nevertheless, at latitudes of 42°N–46°N and from May to October, the magnitude of W_{geo} exceeds that of the difference between W and W_{ekman} so that the combination of W_{ekman} and W_{geo} also overestimate W by about 0.1 m^2/s. In addition, from July to October between 33° and 34°N, the magnitude of W_{geo} exceeds the difference between W and W_{ekman}, so the combination of W_{ekman} and W_{geo} underestimates W by about 0.05 m^2/s. These discrepancies arise because the MLD is less than 30 m along these parts of the coast during summer (Jacox et al. 2018), so that the contribution of geostrophic transport is overestimated when assuming a fixed MLD. The distribution of W_{geo} along the coast from the CESM-LE closely resembles that obtained from a regional ocean model with a much higher horizontal resolution (see Jacox et al., 2018). Marchesiello and Estrade (2010) found that large-scale geostrophic currents are essentially directed onshore, limiting upwelling in subtropical and tropical coastal upwelling zones because of large-scale meridional density gradients that result from the heat flux distribution. Jacox et al. (2018) also noted that geostrophic transport tends to oppose Ekman transport as the alongshore sea level gradient partly balances the alongshore wind stress, although there are places and/or seasons where the mean geostrophic transport does not oppose the mean Ekman transport (e.g., northern CCS).

The anomaly correlation coefficient (ACC) is used to measure the ability of Ekman and geostrophic transports to reproduce interannual variability in coastal upwelling over the years 1920–2100 (Figures 3a and S3a), based on deviations from the monthly climatological means (Figure 2). In general, interannual variability in vertical transport is better captured by the sum of Ekman and geostrophic transports than by Ekman transport alone. For W_{ekman}, an ACC of 0.9 or greater occurs mainly between 34°N and 43°N during January-June and November-December and in some grid cells to the south of 33°N during January-April (Figure 3a). On the other hand, the sum of W_{ekman} and W_{geo} has an ACC with $W > 0.95$ at almost all latitudes and over the full seasonal cycle, indicating the sum captures the overall interannual variability in coastal upwelling extremely well (Figure S3a). The full-field root-mean-square (rms) error, which includes the magnitude of the errors, provides a similar result, as the combination of W_{ekman} and W_{geo} indicates less rms error than W_{ekman} for nearly all latitudes and months (Figures 3b and S3b). During the primary upwelling season (April-October), the combination has a rms error of less than 0.1m^2/s along much of the coast, while W_{ekman} has an error of 0.2–0.5 m^2/s. Further, the transport budget nearly closes during both the early (1925–1954) and late (2071–2100) periods (Figure S4), indicating a minor influence of a changing MLD on our calculations. Indeed, the change in CESM-LE MLD along the United States west coast is under 1 m during the spring/summer upwelling season (not shown).

Figures 3c–3e show the ensemble-mean time series of W, W_{ekman}, W_{geo} and the sum of W_{ekman} and W_{geo} for three selected latitudes/months. For 30.14°N (38.31°N), in September (May), W_{ekman} overestimates W, and W_{geo} has a downwelling-favorable contribution so that the sum of W_{ekman} and W_{geo} matches W, as shown

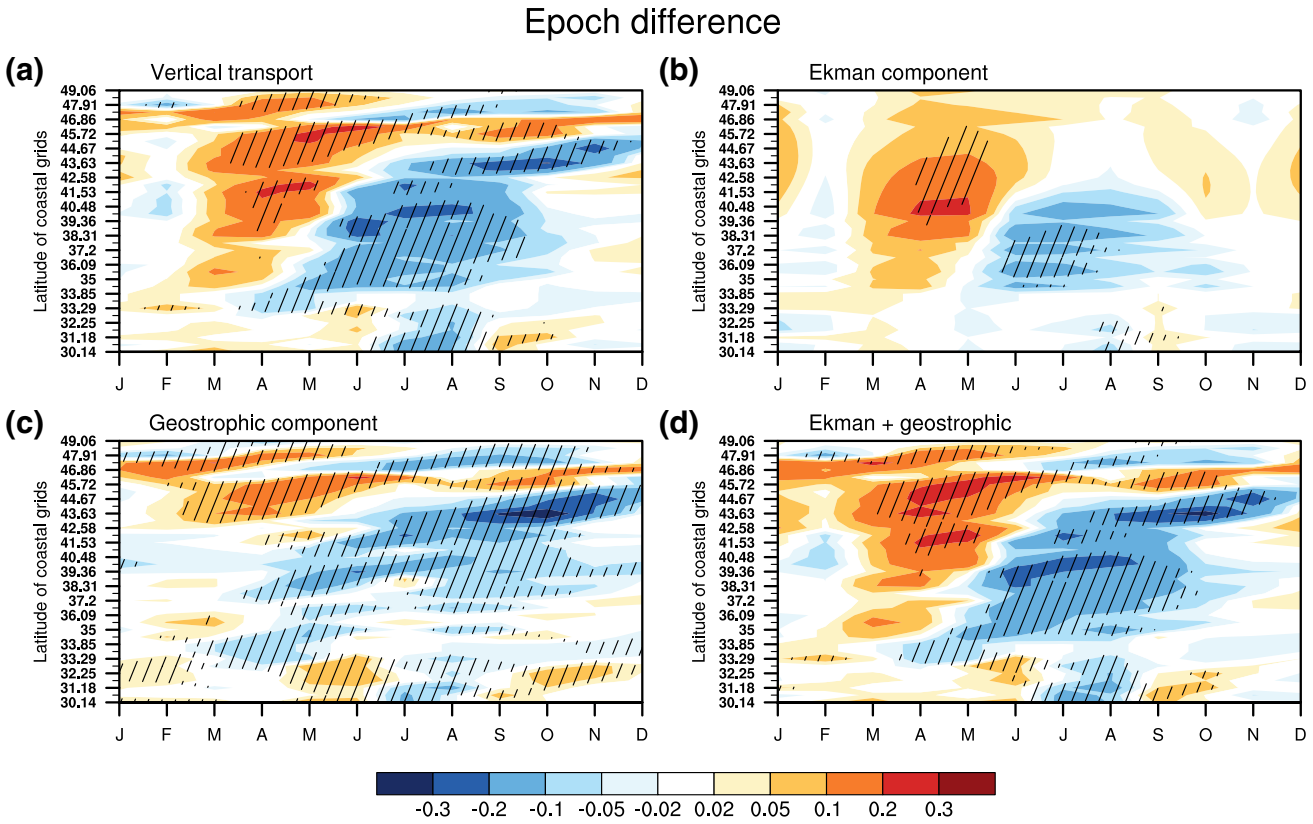

Figure 4. Monthly epoch difference (2071–2100 minus 1925–1954) calculated for (a) vertical transport at 30-m depth (b) Ekman and (c) geostrophic components of the vertical transport, and (d) the combination of the Ekman and geostrophic components. Hatching indicates 95% significance. The unit is m^2/s.

in Figures 3c and 3d. For 47.39°N, in June, W_{ekman} underestimates W, and W_{geo} has an upwelling-favorable contribution so that the sum of W_{ekman} and W_{geo} realistically reproduces W both the mean and interannual variability (Figure 3e).

We now examine the changes driven by greenhouse gas warming (Figure 4). The coastal upwelling response to external radiative forcing by the end of the 21st century varies with latitude and evolves differently in the southern, central and northern parts of the domain. The response is significant at the 95% confidence level in most of the CCS. In particular, the response displays downwelling-favorable changes from June to September along most of the U.S. west coast, except for latitudes 44°N–46°N, where there is enhanced upwelling during this period. From March to May, increased upwelling is projected north of ~39°N. Brady et al., (2017) found similar patterns when analyzing vertical velocity at 50 m depth.

Wind-driven Ekman transport exhibits significant changes under global warming, which contribute to changes in upwelling for certain latitudes and months (Figures 4a and 4b), but the changes in Ekman transport are insufficient to explain all changes in upwelling. For example, W_{ekman} indicates enhanced upwelling in the spring at latitudes of 35°N–49°N and also in early summer north of ~40°N, contributing to the intensified upwelling. However, the change in W_{ekman} underestimates the magnitude of the change in W by 0.05–0.1 m^2/s for grid cells between 43°N and 45°N and near 47°N. Between 35°N and 42°N, W_{ekman} has a downwelling-favorable change of 0.05–0.1 m^2/s during June-September, accounting for only a fraction of the weakened upwelling there. In fact, along most parts of the U.S. west coast, a large portion of the changes in W (0.05–0.2 m^2/s) is unaccounted for by changes in W_{ekman}.

Geostrophic transport-induced upwelling exhibits statistically significant changes off most of the U.S. west coast (Figure 4c). The changes in W_{geo} have a complicated spatial-temporal pattern, with magnitudes of 0.05–0.2 m^2/s, which equal or even exceeds the magnitude of changes in W_{ekman}. For example, W_{geo} displays

an upwelling-favorable change of 0.05–0.1m^2/s from 43°N to 45°N and near 47°N in the spring and early summer, which exceeds the W_{ekman} contribution of ~0.05m^2/s. Changes in W_{geo} intensify upwelling near 46°N but weaken it at 48°N during June-October and at 44°N during July-November. Downwelling-favorable changes in W_{geo} from 36°N to 42°N are 0.05–0.1 m^2/s, comparable to reductions in W_{ekman}. In the southern CCS, geostrophic transport clearly explains a larger fraction of change in upwelling than Ekman transport does. In addition, changes in W_{geo} reproduce the overall difference between W and W_{ekman} in both pattern and magnitude so that the combination of W_{ekman} and W_{geo} nearly matches the changes in W (Figures 4a and 4d).

4. Summary and Discussion

We have examined the respective contributions of Ekman and geostrophic transports to the future change of coastal upwelling in the CCS under greenhouse gas warming. Monthly mean data from the CESM-LE were used, in which forced signals can be separated from internal climate variability. We found that geostrophic transport is an important component of coastal upwelling in the CCS, which is consistent with recent studies (e.g., Jacox et al., 2018). Furthermore, the sum of the Ekman and geostrophic components reproduces the monthly mean climatology and interannual variability of coastal upwelling. We also found significant changes in geostrophic transport in response to greenhouse gas warming along most of the United States west coast, which make a substantial contribution to changes in coastal upwelling, mirroring results from the Peru-Chile upwelling system (Oerder et al., 2015). At some locations in the CCS, changes in upwelling due to geostrophic transport match or even exceed those due to Ekman transport. These results indicate that we must consider geostrophic transport in order to obtain a complete dynamic representation of changes in coastal upwelling due to external radiative forcing.

While changes in Ekman transport are driven primarily by changes in the location and intensity of atmospheric pressure systems (Rykaczewski et al., 2015), changes in geostrophic transport are attributable to changes in the alongshore gradient of SSH under greenhouse warming. Changes in SSH due to external radiative forcing are statistically significant near the United States west coast (Figure S5), and may arise from both local and remote processes, especially those originating in the equatorial Pacific (e.g., Capotondi et al., 2009; Thompson et al., 2014). Furthermore, not just the magnitude of upwelling but also the characteristics of upwelled water, such as nutrient and oxygen content, will likely be altered by future climate change (e.g., Howard et al., 2020). The dynamics of the surface winds, SSH and upwelling in the CCS and their response to climate change warrant further study. Our results clearly indicate that when studying future changes of coastal upwelling under global warming, it is insufficient to consider only the alongshore wind stress, and one must also recognize the importance of ocean circulation.

Data Availability Statement

The CESM-LE data are available at https://www.earthsystemgrid.org/dataset/ucar.cgd.ccsm4.CESM_CAM5_BGC_LE.html. NCEP and ORA-S4 data are available at https://psl.noaa.gov/data/gridded/data.ncep.reanalysis.html and http://icdc.cen.uni-hamburg.de, respectively.

Acknowledgments
This work has been funded by the NOAA Earth System Modeling program. We thank Antonietta Capotondi for her constructive comments. We acknowledge the NCAR climate modeling groups for producing and making available their model output.

References

Bakun, A. (1973). *Coastal upwelling indices, west coast of North America, 1946-71*. US Department of Commerce NOAA Technical Report, NMFS-SSRF.

Bakun, A. (1975). *Daily and weekly upwelling indices, west coast of North America, 1967-73 (No. 693)*. Department of Commerce, National Oceanic and Atmospheric Administration.

Bakun, A. (1990). Global climate change and intensification of coastal ocean upwelling. *Science*, *247*(4939), 198–201. https://doi.org/10.1126/science.247.4939.198

Balmaseda, M. A., Mogensen, K., & Weaver, A. T. (2013). Evaluation of the ECMWF ocean reanalysis system ORAS4. *Quarterly Journal of Royal Meteorological Society*, *139*(674), 1132–1161. https://doi.org/10.1002/qj.2063

Brady, R. X., Alexander, M. A., Lovenduski, N. S., & Rykaczewski, R. R. (2017). Emergent anthropogenic trends in California Current upwelling. *Geophysical Research Letters*, *44*(10), 5044–5052. https://doi.org/10.1002/2017GL072945

Capet, X., Marchesiello, P., & McWilliams, J. (2004). Upwelling response to coastal wind profiles. *Geophysical Research Letters*, *31*(13), L13311. https://doi.org/10.1029/2004GL020123

Capotondi, A., Combes, V., Alexander, M. A., di Lorenzo, E., & Miller, A. J. (2009). Low-frequency variability in the Gulf of Alaska from coarse and eddy-permitting ocean models. *Journal of Geophysical Research*, *114*(C1), C01017. https://doi.org/10.1029/2008JC004983

Cardone, V. J., Greenwood, J. G., & Cane, M. A.. (1990). On trends in historical marine wind data. *Journal of Climate*, *3*(1), 113–127. https://doi.org/10.1175/1520-0442(1990)003⟨0113:OTIHMW⟩2.0.CO;2

Chhak, K., & Di Lorenzo, E. (2007). Decadal variations in the California Current upwelling cells. *Geophysical Research Letters*, *34*(14), L14604. https://doi.org/10.1029/2007GL030203

Colas, F., Capet, X., McWilliams, J. C., & Shchepetkin, A. (2008). 1997–1998 El Niño off Peru: A numerical study. *Programme Oceanography*, *79*(2–4), 138–155. https://doi.org/10.1016/j.pocean.2008.10.015

Deser, C., Phillips, A. S., Alexander, M. A., & Smoliak, B. V. (2014). Projecting North American climate over the next 50 years: Uncertainty due to internal variability. *Journal of Climate*, *27*(6), 2271–2296. https://doi.org/10.1175/JCLI-D-13-00451.1

Deser, C., Phillips, A., Bourdette, V., & Teng, H. (2012). Uncertainty in climate change projections: the role of internal variability. *Climate Dynamics*, *38*(3–4), 527–546. https://doi.org/10.1007/s00382-010-0977-x

Di Lorenzo, E., Schneider, N., Cobb, K., Franks, P., Chhak, K., Miller, A., et al. (2008). North Pacific Gyre Oscillation links ocean climate and ecosystem change. *Geophysical Research Letters*, *35*(8), L08607. https://doi.org/10.1029/2007GL032838

Estrade, P., Marchesiello, P., Verdi`ere, D., A. C., & Roy, C. (2008). Cross-shelf structure of coastal upwelling: A two-dimensional extension of Ekman's theory and a mechanism for inner shelf upwelling shut down. *Journal of Marine Research*, *66*(5), 589–616. https://doi.org/10.1357/002224008787536790

Garcia-Reyes, M., & Largier, J. (2010). Observations of increased wind-driven coastal upwelling off central California. *Journal of Geophysical Research*, *115*(C4), C04011. https://doi.org/10.1029/2009JC005576

Garcia-Reyes, M., Sydeman, W. J., Schoeman, D. S., Rykaczewski, R. R., Black, B. A., Smit, A. J., & Bograd, S. J. (2015). Under pressure: Climate change, upwelling, and eastern boundary upwelling ecosystems. *Frontiers in Marine Science*, *2*, 109. https://doi.org/10.3389/fmars.2015.00109

Howard, E. M., Frenzel, H., Kessouri, F., Renault, L., Bianchi, D., McWilliams, J. C., & Deutsch, C. (2020). Attributing Causes of Future Climate Change in the California Current System With Multimodel Downscaling. *Global Biogeochemical Cycles*, *34*(11), e2020GB006646.

Hsieh, W., & Boer, G. J. (1992). Global climate change and ocean upwelling. *Fisheries Oceanography*, *1*(4), 333–338. https://doi.org/10.1111/j.1365-2419.1992.tb00005.x

Huyer, A. (1983). Coastal upwelling in the California Current system. *Prog. Oceanogr*, *12*(3), 259–284. https://doi.org/10.1016/0079-6611(83)90010-1

Huyer, A., Smith, R. L., & Paluszkiewicz, T. (1987). Coastal upwelling off Peru during normal and El Niño times, 1981-1984. *Journal of Geophysical Research*, *92*(C13), 14297–14307. https://doi.org/10.1029/JC092iC13p14297

Jacox, M. G., & Edwards, C. A. (2011). Effects of stratification and shelf slope on nutrient supply in coastal upwelling regions. *Journal of Geophysical Research: Oceans*, *116*(C3), C03019. https://doi.org/10.1029/2010JC006547

Jacox, M. G., Edwards, C. A., Hazen, E. L., & Bograd, S. J. (2018). Coastal upwelling revisited: Ekman, Bakun, and improved upwelling indices for the US West Coast. *Journal of Geophysical Research*, *123*(10), 7332–7350. https://doi.org/10.1029/2018JC014187

Jacox, M., Moore, A., Edwards, C., & Fiechter, J. (2014). Spatially resolved upwelling in the California Current System and its connections to climate variability. *Geophysical Research Letters*, *41*(9), 3189–3196. https://doi.org/10.1002/2014GL059589

Kalnay, E., Kanamitsu, M., Kistler, R., Collins, W., Deaven, D., & Gandin, L., et al. (1996). The NCEP/NCAR 40-year reanalysis project. *The Bulletin of the American Meteorological Society*, *77*(3), 437–472. https://doi.org/10.1175/1520-0477(1996)077<0437:TNYRP>2.0.CO;2

Kay, J. E., Deser, C., Phillips, A., Mai, A., Hannay, C., Strand, G., et al. (2015). The Community Earth System Model (CESM) large ensemble project: A community resource for studying climate change in the presence of internal climate variability. *Bulletin of the American Meteorological Society*, *96*(8), 1333–1349. https://doi.org/10.1175/BAMS-D-13-00255.1

Large, W., & Danabasoglu, G. (2006). Attribution and impacts of upper-ocean biases in CCSM3. *Journal of Climate*, *19*(11), 2325–2346. https://doi.org/10.1175/JCLI3740.1

Lentz, S. J., & Chapman, D. C. (2004). The importance of nonlinear cross-shelf momentum flux during wind-driven coastal upwelling. *Journal of Physical Oceanography*, *34*(11), 2444–2457.

Li, W., Li, L., Ting, M., & Liu, Y. (2012). Intensification of Northern Hemisphere subtropical highs in a warming climate. *Nature Geoscience*, *5*(11), 830–834. https://doi.org/10.1038/ngeo1590

Lovenduski, N. S., McKinley, G. A., Fay, A. R., Lindsay, K., & Long, M. C. (2016). Partitioning uncertainty in ocean carbon uptake projections: Internal variability, emission scenario, and model structure. *Global Biogeochemical Cycles*, *30*(9), 1276–1287. https://doi.org/10.1002/2016GB005426

Marchesiello, P., & Estrade, P. (2010). Upwelling limitation by onshore geostrophic flow. *Journal of Marine Research*, *68*(1), 37–62. https://doi.org/10.1357/002224010793079004

McCreary, J. P., Shetye, S. R., & Kundu, P. K. (1986). Thermohaline forcing of eastern boundary currents: With application to the circulation off the west coast of Australia. *Journal of Marine Research*, *44*(1), 71–92. https://doi.org/10.1357/002224086788460184

Mote, P. W., & Mantua, N. J. (2002). Coastal upwelling in a warmer future. *Geophysical Research Letters*, *29*(23), 53. https://doi.org/10.1029/2002GL016086

Narayan, N., Paul, A., Mulitza, S., & Schulz, M. (2010). Trends in coastal upwelling intensity during the late 20th century. *Ocean Science Discussions*, *7*(1), 815–823.

Oerder, V., Colas, F., Echevin, V., Codron, F., Tam, J., & Belmadani, A. (2015). Peru-Chile upwelling dynamics under climate change. *Journal of Geophysical Research*, *120*(2), 1152–1172. https://doi.org/10.1002/2014JC010299

Riahi, K., Rao, S., Krey, V., Cho, C., Chirkov, V., Fischer, G., & Rafaj, P. (2011). RCP 8.5-A scenario of comparatively high greenhouse gas emissions. *Climate Dynamics*, *109*(1–2), 33. https://doi.org/10.1007/s10584-011-0149-y

Rossi, V., Feng, M., Pattiaratchi, C., Roughan, M., & Waite, A. M. (2013). On the factors influencing the development of sporadic upwelling in the Leeuwin Current system. *Journal of Geophysical Research: Oceans*, *118*(7), 3608–3621. https://doi.org/10.1002/jgrc.20242

Rykaczewski, R. R., & Checkley, D. M. (2008). Influence of ocean winds on the pelagic ecosystem in upwelling regions. *Proceedings of the National Academy of Sciences*, *105*(6), 1965–1970. https://doi.org/10.1073/pnas.0711777105

Rykaczewski, R. R., Dunne, J. P., Sydeman, W. J., Garćıa-Reyes, M., Black, B. A., & Bograd, S. J. (2015). Poleward displacement of coastal upwelling-favorable winds in the ocean's eastern boundary currents through the 21st century. *Geophysical Research Letters*, *42*(15), 6424–6431. https://doi.org/10.1002/2015GL064694

Ryther, J. H. (1969). Photosynthesis and fish production in the sea. *Science*, *166*(3901), 72–76. https://doi.org/10.1126/science.166.3901.72

Smith, R., Jones, P., Briegleb, B., Bryan, F., Danabasoglu, G., & Dennis, J., et al. (2010). The parallel ocean program (POP) reference manual: ocean component of the community climate system model (CCSM) and community earth system model (CESM). *LAUR-01853*, *141*, 1–140.

Sydeman, W., Garcia-Reyes, M., Schoeman, D., Rykaczewski, R., Thompson, S., Black, B., & Bograd, S. (2014). Climate change and wind intensification in coastal upwelling ecosystems. *Science*, *345*(6192), 77–80. https://doi.org/10.1126/science.1251635

Thompson, P. R., Merrifield, M. A., Wells, J. R., & Chang, C. M. (2014). Wind-driven coastal sea level variability in the northeast Pacific. *Journal of Climate*, *27*(12), 4733–4751. https://doi.org/10.1175/JCLI-D-13-00225.1

Veitch, J., Penven, P., & Shillington, F. (2010). Modeling equilibrium dynamics of the Benguela Current System. *Journal of Physical Oceanography*, *40*(9), 1942–1964. https://doi.org/10.1175/2010JPO4382.1

Wang, D., Gouhier, T. C., Menge, B. A., & Ganguly, A. R. (2015). Intensification and spatial homogenization of coastal upwelling under climate change. *Nature*, *518*(7539), 390–394. https://doi.org/10.1038/nature14235

Xiu, P., Chai, F., Curchitser, E. N., & Castruccio, F. S. (2018). Future changes in coastal upwelling ecosystems with global warming: The case of the California Current System. *Scientific Reports*, *8*(1), 2866. https://doi.org/10.1038/s41598-018-21247-7

Yin, J. (2012). Century to multi-century sea level rise projections from CMIP5 models. *Geophysical Research Letters*, *39*(17), L17709. https://doi.org/10.1029/2012GL052947

Yin, J., Griffies, S. M., & Stouffer, R. J. (2010). Spatial variability of sea level rise in twenty-first century projections. *Journal of Climate*, *23*(17), 4585–4607. https://doi.org/10.1175/2010JCLI3533.1

References from the Supporting Information

Balmaseda, M. A., Mogensen, K., & Weaver, A. T. (2013). Evaluation of the ECMWF ocean reanalysis system ORAS4. *Quarterly Journal of Royal Meteorological Society*, *139*(674), 1132–1161. https://doi.org/10.1002/qj.2063

Kalnay, E., Kanamitsu, M., Kistler, R., Collins, W., Deaven, D., & Gandin, L., et al. (1996). The NCEP/NCAR 40–year reanalysis project. *The Bulletin of the American Meteorological Society*, *77*(3), 437–472. https://doi.org/10.1175/1520-0477(1996)077<0437:TNYRP>2.0.CO;2